ARTICLE

Spectroscopic Identification and Bonding Properties of $HNCOCa^+$: a Matrix Isolation and Computational Study†

Xin Jiang, Beibei Sun, Guanjun Wang, Lina Wang*, Xiaoqing Zeng*, Mingfei Zhou*

Department of Chemistry, Shanghai Key Laboratory of Molecular Catalysis and Innovative Materials, Fudan University, Shanghai 200438, China

(Dated: Received on February 9, 2024; Accepted on March 4, 2024)

Metal (iso)cyanides dominate the molecular inventory of metal-bearing species in the interstellar medium. Their oxide counterparts, metal (iso)cyanates, have potential as interstellar molecules and have received significant attention. However, cationic complexes $HNCOM^+$ as precursors to metal (iso)cyanates are rarely studied. Herein, we investigated $HNCOCa^+$ by exploiting infrared spectrometry with isotopic substitutions and quantum chemical calculations. For comparison, the light and heavy alkaline earth metal cationic complexes $HNCOBe^+$ and $HNCOBa^+$ were also explored. $HNCOCa^+$ and $HNCOBe^+$ rather than $HNCOBa^+$ can be experimentally generated by the reactions of metal cations with HNCO. The observed antisymmetric and symmetric NCO stretching vibrations in $HNCOCa^+$ (2362.6 and 1330.4 cm^{-1}) are higher than those in free HNCO (2268.5 and 1320.3 cm^{-1}) but lower than those in $HNCOBe^+$ (2426.4 and 1355.2 cm^{-1}). These shifts can be explained by the charge polarization within the NCO fragment in $HNCOBe^+$ and $HNCOCa^+$. Bonding analysis suggests that HNCO–Be^+ bond favors covalent character (54%) while HNCO–Ca^+ bond has higher electrostatic character (57%). The dominant electrostatic interaction (64%) in HNCO–Ba^+ bond results in the low bond energy, which might account for its absence in experiments.

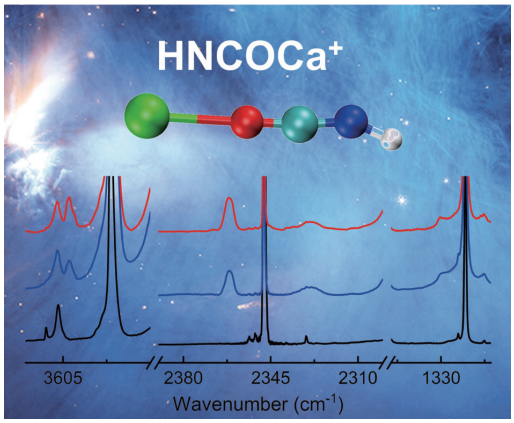

Key words: Calcium, HNCO, Bonding analysis, Matrix isolation, Vibrational spectroscopy

I. INTRODUCTION

Metal-bearing molecules are essential components of the interstellar medium (ISM), providing crucial insights into the ionization balance, elemental abundances, nucleosynthesis processes, and dust grain formation in diverse astrophysical environments [1–3]. Among the nearly thirty metal-bearing species detected in the ISM, metal cyanides and isocyanides are particularly prominent [4–14]. Models explaining the formation of these metal-(iso)cyanide molecules in the outer shells of asymptotic giant branch star IRC+10216, propose a two-step mechanism involving the radiative association of cyanopolyynes ($HC_{2n+1}N$) with the metal ion (M^+) and the subsequent dissociative recombination of the corresponding complex $HC_{2n+1}NM^+$ with electrons (Eq.(1) and Eq.(2)) [15]. The complex cations $HC_{2n+1}NM^+$ have been proposed as the key intermediates, and the abundance of metal-(iso)cyanide com-

† Part of Special Issue "In Memory of Prof. Qihe Zhu on the occasion of his 100th Anniversary".

* Authors to whom correspondence should be addressed. E-mail: lina_wang@fudan.edu.cn, xqzeng@fudan.edu.cn, mfzhou@fudan.edu.cn

pounds depends on the branching ratios of different fragmentation channels during dissociative recombination. This model has explained the abundances of the detected species such as MgCN, MgNC, HMgNC and MgC_3N [16].

$$M^+ + HC_{2n+1}N \rightarrow HC_{2n+1}NM^+ + h\nu \quad (1)$$

$$HC_{2n+1}NM^+ + e \rightarrow \begin{cases} MC_{2n+1}N + H \\ MNC_{2n+1} + H \end{cases} \quad (2)$$

As the simplest molecules including carbon and nitrogen, both cyanide (CN) and isocyanate (NCO) radicals are known in astronomical environments. The oxidation of CN by O_3 or OH radical has been demonstrated to generate NCO [17, 18]. The study of molecules containing the NCO backbone, such as peptide-bond-bearing molecules, has been deeply ingrained in understanding the evolution of prebiotic chemistry [19–23]. While there has been significant exploration of metal (iso)cyanides, there are limited theoretical data available for metal-(iso)cyanates, which hinders their characterization in space and the understanding of their role in interstellar chemistry. Although some previous theoretical studies have investigated LiNCO [24, 25], CaNCO [26], and HBeNCO [27], recent high-level *ab initio* spectroscopic predictions have provided insights into the spectroscopic parameters and electronic structures of the AlNCO [28], NaNCO [4], MgNCO [29], and HMgNCO [30] isomers. In analogy with the aforementioned mechanism (Eq.(1) and Eq.(2)), the cationic molecules $HNCOM^+$ could be the precursor of metal-(iso)cyanates. The formation process of HNCO has received significant attention and the cationic complexes H_2NCO^+ and $HNCOH^+$ have been proposed to be involved in [13, 31, 32]. The dissociative recombination of H_2NCO^+ was first proposed as a potential source of HNCO in the Taurus molecular cloud (TMC-1) as far back as 1981 [33, 34]. Furthermore, chemical models have included H_2NCO^+ in the gas phase synthesis of HNCO (Eq.(3)) [13]. In addition, the other less-stable cationic form $HNCOH^+$ was also assumed to be the precursor of HNCO and HOCN (Eq.(4)) [20].

$$H_2NCO^+ + e \rightarrow HNCO + H \quad (3)$$

$$HNCOH^+ + e \rightarrow \begin{cases} HOCN + H \\ HNCO + H \end{cases} \quad (4)$$

Alkaline earth metals, particularly calcium (Ca), are significant constituents of the interstellar medium, and their abundance is heavily depleted in dense clouds, making them a major component of interstellar dust [35, 36]. These metals have a high affinity with oxygen, allowing them to form stable oxides and play a crucial role in stellar interiors. Investigating bonding behavior of alkaline earth metals has provided valuable insights into the related chemical processes in the ISM and how they impact the formation and evolution of stars and planets. Recent studies have revealed diverse bonding interactions of alkaline earth metals [37, 38], such as the bonding situation in alkaline earth-octacarbonyl complexes $M(CO)_8$ (M = Ca, Sr, and Ba), which demonstrate that alkaline earth metals can mimic transition metals and effectively utilize their $(n-1)$d atomic orbitals in chemical bonding [37]. In addition, bonding analyses of the linear HNBeCO complex have shown an unprecedented triple bond consisting of a dative σ bond and two degenerate electron-sharing π bonds [38]. The rich bonding properties of alkaline earth metals dictate their reactivity, reaction mechanisms, and stability ranges. Herein, we investigated the cationic complex $HNCOCa^+$ from both experimental and theoretical point of view. In addition, the light and heavy alkaline earth metal cationic complexes $HNCOBe^+$ and $HNCOBa^+$ were also explored for comparison. The complexes $HNCOCa^+$ and $HNCOBe^+$ rather than $HNCOBa^+$ can be experimentally generated and spectroscopically detected. The quantum chemical calculations explore the interesting geometries and bonding interactions, and the results are in good agreement with the experimental observation.

II. EXPERIMENTS AND CALCULATIONS

A. Experimental methods

A Nd:YAG laser (Continuum, Minilite II) operating at a 1064 nm fundamental wavelength, with a repetition rate of 10 Hz and a pulse width of 6 ns, was utilized to ablate a rotating metal target and generate metal atoms. A cryogenic gold-plated copper block matrix support, maintained at 3 K using a closed-cycle helium refrigerator, was utilized for the co-deposition of laser-evaporated metal atoms with HNCO in excess neon. The HNCO/Ne mixtures were prepared in a stainless-steel vacuum line using a standard manometric technique. Following a 30-min sample deposition at 3 K, mid-infrared absorption spectra in the range of

DOI: 10.1063/1674-0068/cjcp2402019

4000–450 cm^{-1} were recorded using a Bruker Vertex 70 V spectrometer. The spectra were acquired at a resolution of 0.5 cm^{-1} with a liquid nitrogen-cooled broad band HgCdTe (MCT) detector. The samples were subjected to annealing at the desired temperatures and subsequently cooled back to 3 K before acquiring the spectra. In the case of selected samples, photo-excitation experiments were conducted through a quartz window mounted on the assembly. Isocyanic acid HNCO was prepared following the procedures reported in the literature [39]. Isotopically-labeled samples, namely $HN^{13}CO$ and $H^{15}NCO$, were prepared using the ^{13}C and ^{15}N-labeled potassium cyanates through reactions of potassium phenoxide with ^{13}C and ^{15}N-labeled urea, following the procedures described in the literature [40].

B. Theoretical methods

The geometry optimization and vibrational spectra of HNCO and $HNCOM^+$ (M = Be, Ca, or Ba) were calculated at the B3LYP level of theory. The used basis sets were 6-311+G(3df) [41, 42] for H, N, C, O, Be, and Ca atoms, and D95V basis sets [43] combined with the Stuttgart/Dresden relativistic effective core potentials (SDD) [44] for Ba atom. The calculated vibrational frequencies were scaled by 0.967 as suggested in the literature [45]. All calculations were performed using Gaussian 16 [46]. The quantum theory of atoms in molecules (QTAIM) method developed by Bader [47] was carried out with the AIMALL program [48]. The NBO calculations were performed using version 6.0 [49]. The bonding situation in the $HNCOM^+$ (M = Be, Ca, and Ba) complex was further analyzed using the EDA-NOCV (energy decomposition analysis in combination with natural orbitals for chemical valence) method [50, 51]. Details of the method have been described in the literatures [52, 53]. These calculations were performed using the ADF 2014.10 program package [54, 55]. For Be and Ca systems, EDA-NOCV calculations were carried out at the BP86/TZ2P [56] level, while for the Ba system, the calculations were performed at the M06-2X/TZ2P level, using the B3LYP/6-311+G(3df) optimized geometry.

III. RESULTS AND DISCUSSION

Laser-ablation was exploited to generate metal atoms, ions, and electrons which subsequently deposit with HNCO in excess neon at 3 K to prepare $HNCOM^+$ (M = Be, Ca, and Ba) cation complexes [57]. In the reaction of Ca^+ cation with HNCO, the spectra in the 3620–3580, 2390–2310 and 1340–1310 cm^{-1} regions are of particular interest and shown in FIG. 1. After sample deposition at 3 K, a group of product absorptions at 3603.2, 2362.6, and 1330.4 cm^{-1} (labeled **a**) in experiment were observed. However, they were completely destroyed upon irradiation at 625 nm. The experimental procedure was repeated using isotopically labeled $HN^{13}CO$ and $H^{15}NCO$ samples (FIG. 2), as well as mixtures of HNCO + $HN^{13}CO$ (1:1) and HNCO + $H^{15}NCO$ (1:1). The band at 2362.6 cm^{-1} shifts to 2299.3 cm^{-1} with the $HN^{13}CO$ sample and to 2348.8 cm^{-1} with the $H^{15}NCO$ sample. These shifts in isotopic frequencies clearly indicate that the 2362.6 cm^{-1} band corresponds to the antisymmetric NCO stretching mode, which is 94.1 cm^{-1} higher than that of the free HNCO molecule (2268.5 cm^{-1}). The band at 1330.4 cm^{-1} exhibits a large shift of −14.7 cm^{-1} for the ^{15}N isotope, but only a small shift of −1.2 cm^{-1} for the ^{13}C isotope, as shown in Table I. This band can be assigned to the mode of the NCO symmetric stretching vibration. The 3603.2 cm^{-1} band shifts to 3591.9 cm^{-1} with $H^{15}NCO$, which is indicative of a N−H stretching mode [58]. Note that upon ^{13}C isotope labeling, this band splits into two bands at 3622.7 and 3597.4 cm^{-1}, which might be attributed to the Fermi resonance with the combination tone of the antisymmetric and symmetric NCO stretching modes.

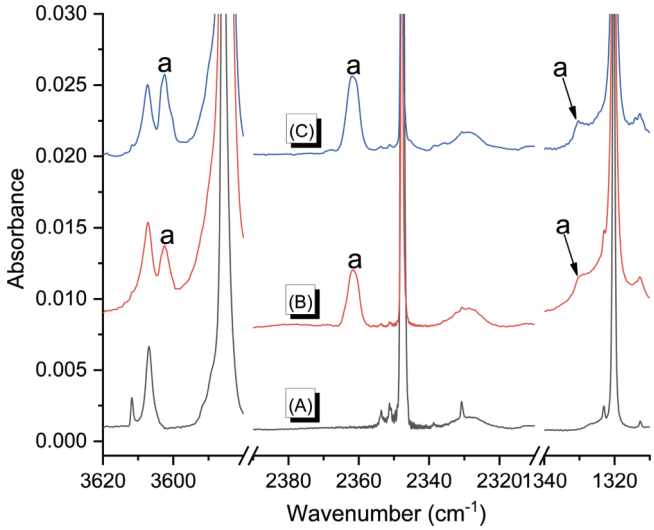

FIG. 1 Infrared spectra in the 3620–3580, 2390–2310 and 1340–1310 cm^{-1} regions after 30 min of sample deposition at 3 K in neon. (A) Pure 0.05% HNCO deposition; co-deposition of laser-ablated calcium atoms with 0.05% HNCO (B) or 0.05% HNCO doped with CCl_4 (C). The IR bands of $HNCOCa^+$ (labeled **a**) are indicated.

DOI: 10.1063/1674-0068/cjcp2402019

TABLE I Observed and calculated IR frequencies and isotopic shifts ($\Delta\nu$) of $HNCOCa^+$.

Frequency/cm^{-1}		$\Delta\nu(^{13}C)/cm^{-1}$		$\Delta\nu(^{15}N)/cm^{-1}$		Assignment
Obs.[a]	Calc.[b]	Obs.[a]	Calc.[b]	Obs.[a]	Calc.[b]	
3603.2	3647.7 (709)	19.5/−5.8	−0.6	−11.3	−11.5	ν(HN)
2362.6	2353.5 (1069)	−63.3	−64.9	−13.8	−14.1	ν_{asym}(NCO)
1330.4	1321.4 (155)	−1.2	−0.8	−14.7	−17.3	ν_{sym}(NCO)
	589.1 (<1)		−15.1		−1.1	δ(NCO)
	587.1 (2)		−15.6		−1.5	δ(NCO)

[a] Observed band positions in neon matrix at 3 K.
[b] Calculated IR harmonic frequencies (cm^{-1}), intensities (km/mol, in parentheses), and isotopic shifts $\Delta\nu$ (cm^{-1}) at the B3LYP/6-311+G(3df) level of theory. The calculated frequencies are scaled by a factor of 0.967.

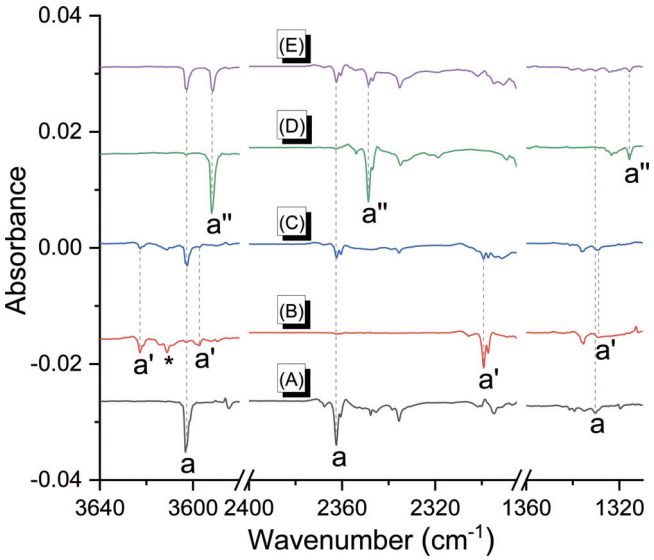

FIG. 2 IR difference spectra in the 3640–3580, 2400–2285 and 1360–1310 cm^{-1} regions from co-deposition of laser-ablated calcium atoms with 0.05% HNCO in neon (spectra taken after 2 min of 625 nm irradiation minus the spectra taken after 11 K annealing). (A) 0.05% HNCO, (B) 0.05% $HN^{13}CO$, (C) 0.05% $HN^{12}CO$+0.05% $HN^{13}CO$, (D) 0.05% $H^{15}NCO$, and (E) 0.05% $H^{14}NCO$+0.05% $H^{15}NCO$. The IR bands of $HNCOCa^+$ (labeled **a**), $HN^{13}COCa^+$ (labeled **a'**), $H^{15}NCOCa^+$ (labeled **a''**) and the unknown species (*) are indicated.

The spectra obtained from experiments using mixed $HN^{12}CO+HN^{13}CO$ (1:1) and $H^{14}NCO+H^{15}NCO$ (1:1) isotopic samples provide clear evidence that species a consists of only one NCO moiety and one NH subunit (FIG. 2). The observation of the blue-shifted antisymmetric and symmetric NCO stretching modes (FIG. 1) indicates that the HNCO molecule is coordinated in an end-on fashion to a positively charged metal center. Consequently, the group bands at 3603.2, 2362.6, and 1330.4 cm^{-1} are assigned to a $HNCOCa^+$ cation complex. To confirm this cation assignment, an additional experiment was conducted by introducing CCl_4 as an electron trap [59, 60]. The infrared spectra obtained from two parallel experiments, one with CCl_4 doping and the other without, were compared (FIG. 1 (B) and (C)). The spectra clearly demonstrate that the intensities of the group absorptions increase upon the addition of a trace amount of CCl_4.

The similar group absorptions (3542.6, 2426.4 and 1355.2 cm^{-1}) [38] have been observed as a side product in our previous study on the reaction of HNCO and laser-ablated Be atom (FIG. S1 in Supplementary materials, SM), and other products have already been explored. In the present study, we re-optimized the experimental conditions for generating this group absorption bands and performed the isotopic-labeled experiments. The corresponding isotopic shifts of these bands resemble those of $HNCOCa^+$ absorptions (FIG. S2 in SM), which further confirms that they can be assigned to the fundamental vibrational modes of $HNCOBe^+$. Note that the antisymmetric and symmetric NCO stretching modes in $HNCOBe^+$ (2426.4 and 1355.2 cm^{-1}) are higher than those in $HNCOCa^+$ (2362.6 and 1330.4 cm^{-1}) and exhibit larger blue-shifts with 157.9 and 34.9 cm^{-1} from that of free HNCO (2268.5 and 1320.3 cm^{-1}).

Table I and Table S1 in SM show the experimental and calculated IR spectra values for $HNCOCa^+$ and $HNCOBe^+$, respectively. The computed frequency shifts $\Delta\nu$ of $HNCOCa^+$ and $HNCOBe^+$ match the measured value well. For comparison, the calculated IR spectra values for $HNCOBa^+$ are also given in Table S1 (SM). The antisymmetric NCO stretching vibration in $HNCOBa^+$ calculated at near 2330.0 cm^{-1} is the strongest mode. In contrast to the observation in Ca and Be experiments, the nonexistence of this band in the spectrum eliminates the possibility of $HNCOBa^+$ formation during the experiments (FIG. S1 in SM).

FIG. 3 shows the calculated equilibrium geometries

DOI: 10.1063/1674-0068/cjcp2402019

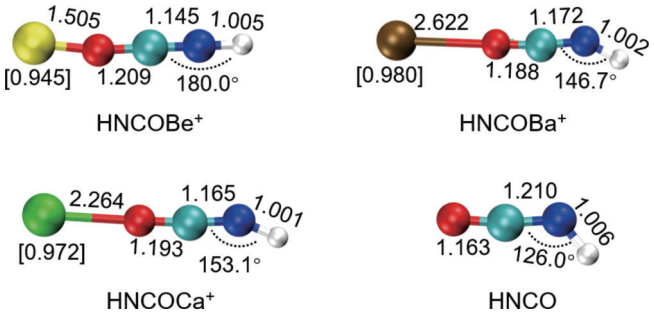

FIG. 3 Calculated equilibrium geometries of HNCOM$^+$ (M=Be, Ca, and Ba) and HNCO at the B3LYP/6-311+G(3df) level of theory. Bond lengths and angles are in Å and degree, respectively. The calculated spin density (e) is given in square brackets.

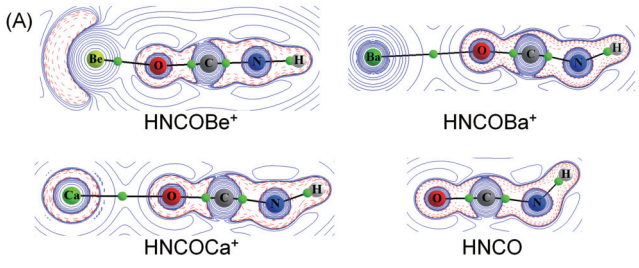

(B)

		HNCOBe$^+$	HNCOCa$^+$	HNCOBa$^+$	HNCO
NBO	N	−0.49	−0.60	−0.62	−0.76
	C	0.94	0.90	0.89	0.85
	O	−0.90	−0.76	−0.72	−0.49
	M	0.97	0.99	0.99	

FIG. 4 (A) Laplacian distribution at the B3LYP/6-311+G(3df) level of theory. Blue lines show areas of charge depletion ($\nabla^2\rho(r)>0$) while red lines indicate areas of charge concentration ($\nabla^2\rho(r)<0$). The bond paths are represented by solid lines connecting the atomic nuclei, and the bond critical points are depicted as green dots. (B) Calculated partial natural charges given by NBO.

and the theoretically predicted bond angles and lengths of HNCOM$^+$ (M = Be, Ca, and Ba) and HNCO. The computed value for the HNC bending angle of 126° in HNCO has parallels with the early identified H−N=C=O bonding character [61]. By comparison, the calculation suggests that HNCOBe$^+$ has a quasi-linear structure with a H−N−C angle of 180.0°. The calculated N−C distance of 1.145 Å in HNCOBe$^+$ is significantly shorter than that in HNCO (1.210 Å) and aligns with the standard value of 1.14 Å for a N≡C triple bond proposed by Pyykkö and Atsumi [62]. In addition, the C−O distance of 1.209 Å in HNCOBe$^+$ becomes longer than that in HNCO (1.163 Å). Therefore, the bond character of HNCOBe$^+$ can be sketched as H−N≡C−O−Be$^+$. The strengthened NC bond while weakened CO bond agree with the large blue-shifts of the antisymmetric and symmetric NCO stretching vibrations. Compared with HNCOBe$^+$, HNC angles in HNCOCa$^+$ and HNCOBa$^+$ gradually bend (153.1° and 146.7°) along with the lengthened N−C bond (1.165 and 1.172 Å) and shortened C−O bond (1.193 and 1.188 Å). The HN bond in HNCOCa$^+$ (1.001) is slightly shorter than that in HNCOBe$^+$ (1.005) and HNCO (1.006), consistent with the higher frequency observed for the ν(HN) mode in HNCOCa$^+$ (3603.2 cm^{-1}) compared to HNCOBe$^+$ (3542.6 cm^{-1}) and HNCO (3538.1 cm^{-1}). FIG. 3 also presents the spin density distribution in HNCOM$^+$, illustrating the localization of the unpaired electron at the metal atom.

The Laplacian distribution depicted in FIG. 4 highlights the local charge concentration ($\nabla^2\rho(r)<0$, red lines) at the terminal side of metal in HNCOM$^+$. It clearly shows that charge concentration is significant at Be atom in HNCOBe$^+$ and gradually reduces from Be to Ba system. Especially, those at Ba atom are nearly negligible. The partial natural charges given by NBO suggest that the HNCO moiety possesses near-neutral character, as shown in FIG. 4(B). The bonding between the metal cation M$^+$ and the oxygen atom induces minimal charge migration between the two moieties, but it does cause an internal charge migration from the nitrogen to the oxygen atom within the HNCO fragment. The change of the N→O charge distribution would strengthen the N−C bond and weaken the C−O bond. The charge migration quantity for HNCOCa$^+$ is between those of HNCOBe$^+$ and HNCOBa$^+$, which can explain the experimental observation that the associated antisymmetric and symmetric NCO stretching vibrations in HNCOCa$^+$ are lower than those in HNCOBe$^+$.

We analyzed the bonding situation with the energy decomposition analysis in combination with natural orbitals for chemical valence (EDA-NOCV) approaches. The numerical results of the EDA-NOCV calculations of HNCOM$^+$ have been shown in Table II and Tables S2 and S3 (SM). The calculated values suggest that the HNCO−Be$^+$ bond has a higher covalent character (54%) than electrostatic character (46%). For HNCOCa$^+$ and HNCOBa$^+$ system, the percentage contribution of orbital interaction gradually decreases and electrostatic interactions become dominant (57% and 64%). The change of the bonding in the HNCO−M$^+$ systems corresponds to the alteration of the bonding between nitrogen and oxygen, leading to an increase in the angle of HNC from 126° in HNCO to 147°, 153°, and 180° for

DOI: 10.1063/1674-0068/cjcp2402019

TABLE II Calculated bond dissociation energies and EDA-NOCV results (kcal/mol) for HNCO–M^+ complexes in $HNCOM^+ \rightarrow HNCO$ (S)+M^+ (D), here fragments are given in singlet (S) or doublet (D).

M	$\Delta H_{0\,K}$[a]	$\Delta G_{298\,K}$[a]	ΔE_{orb}[b]	ΔE_{elstat}[b]
Be	60.4	53.9	−96.1 (54%)	−80.4 (46%)
Ca	25.3	18.8	−31.1 (43%)	−41.6 (57%)
Ba	18.3	12.3	−19.0 (36%)	−34.5 (64%)

[a] The $\Delta H_{0\,K}$ data include the corrections by zero-point vibrational energies and the $\Delta G_{298\,K}$ values consider the thermodynamic and vibrational corrections at 298 K.
[b] The percentage values in parentheses indicate the contribution to the overall attractive interactions $\Delta E_{orb}+\Delta E_{elstat}$.

Ba, Ca, and Be-bound HNCO, respectively. Correspondingly, the bond dissociation energies for bond rupture $HNCOM^+ \rightarrow M^+ + HNCO$ have a declining trend (Table II). The weak barium-oxygen bond is consistent with the Ba–O distance of 2.622 Å in optimized HNCO-Ba^+ (FIG. 3), which is even longer than the standard value for a Ba–O single bond length (2.59 Å). The low bond dissociation energy of $HNCOBa^+$ might account for its absence in experiment.

Calcium isocyanide CaNC has been detected in IRC+10216 [12]. Its hydride HCaNC and oxide CaNCO and their isomers have been theoretically investigated for the electronic structures and spectroscopic parameters [63], which aims to help an eventual interstellar detection. Herein, the dissociative recombination of $HNCOCa^+$ with electron to produce Ca-bearing molecules was computationally explored (Table III). The fragmentation channel of CaNCO and H atom is the most energetically favored process (ΔH = −104.8 kcal/mol), while the dissociation into the isomer CaOCN and H atom is less exothermic and releases 90.3 kcal/mol. The ΔH of decomposition into CaNC and CaCN were calculated to be −69.5 and −64.5 kcal/mol, while the fragmentation for generating the hydrides HCaNC and HCaCN only releases 27.1 and 22.7 kcal/mol. The energy analysis highlights the key intermediate nature of the cationic complex $HNCOCa^+$ in formation of CaNCO or CaOCN, which provides implication on the presence of calcium (iso)cyanates in the ISM.

IV. CONCLUSION

In summary, we explored the cationic complex HN-

TABLE III Calculated reaction energies ($\Delta H_{0\,K}$, kcal/mol) for the possible dissociative recombination of $HNCOCa^+$ with electron.

Product	$\Delta H_{0\,K}$	Product	$\Delta H_{0\,K}$
CaNCO+H	−104.8	CaCN+OH	−64.5
CaOCN+H	−90.3	HCa+NCO	−53.6
CaO+HCN	−96.0	CaOH+CN	−46.4
CaO+HNC	−82.3	HCaNC+O	−27.1
CaNC+OH	−69.5	HCaCN+O	−22.7

COM^+ (M = Be, Ca, and Ba) by the reaction of laser-ablated metal cations with HNCO, in which $HNCOBe^+$ and $HNCOCa^+$ were identified while $HNCOBa^+$ was not observed. The dominant features in the infrared (IR) spectra of $HNCOBe^+$ and $HNCOCa^+$ are the intense bands related to the antisymmetric NCO stretching modes, which will likely make observation of these systems easier with space-based IR. The quantum-chemical calculations reveal that the $HNCO \rightarrow Be^+$ donation results in strong binding due to the orbital interactions and a significant charge polarization within the NCO fragment. From $HNCOBe^+$ to $HNCOCa^+$ and $HNCOBa^+$, the contribution of orbital interaction and the degree of polarization gradually decreases. The absence of $HNCOBa^+$ in experiment would result from the low bond energy. The stability analysis of the cationic complexes $HNCOM^+$ might help understand the chemical processes of the related metal-bearing molecules in astrochemistry.

Supplementary materials: Details on additional infrared spectra and numerical calaulations for HN-$COBe^+$, $HNCOCa^+$ and $HNCOBa^+$ are shown.

V. NOTES

The authors declare no competing financial interests.

VI. ACKNOWLEDGMENTS

This work was supported by the National Natural Science Foundation of China (No.22025301, No.22273012, and No.22321003).

[1] R. C. Fortenberry, Mol. Astrophys. **18**, 100062 (2020).
[2] A. Potapov and M. McCoustra, Int. Rev. Phys. Chem. **40**, 299 (2021).

[3] A. Mortier, N. C. Santos, S. Sousa, G. Israelian, M. Mayor, and S. Udry, Astron. Astrophys. **551**, A112 (2013).
[4] M. Sanz-Novo, P. Ortega, P. Redondo, A. Largo, J. L. Alonso, and C. Barrientos, Astrophys. J. **941**, 40 (2022).
[5] V. J. Esposito, T. Trabelsi, and J. S. Francisco, Astrophys. J. **924**, 139 (2022).
[6] T. Trabelsi, O. Sghaier, H. Ferjani, and J. S. Francisco, Astron. Astrophys. **672**, A79 (2023).
[7] M. Guélin, R. Lucas, and J. Cernicharo, Astron. Astrophys. **280**, L19 (1993).
[8] L. M. Ziurys, A. J. Apponi, M. Guélin, and J. Cernicharo, Astrophys. J. **445**, L47 (1995).
[9] J. L. Highberger, C. Savage, J. H. Bieging, and L. M. Ziurys, Astrophys. J. **562**, 790 (2001).
[10] L. M. Ziurys, C. Savage, J. L. Highberger, A. J. Apponi, M. Guélin, and J. Cernicharo, Astrophys. J. **564**, L45 (2002).
[11] M. Guélin, S. Muller, J. Cernicharo, M. C. McCarthy, and P. Thaddeus, Astron. Astrophys. **426**, L49 (2004).
[12] J. Cernicharo, L. Velilla-Prieto, M. Agúndez, J. R. Pardo, J. P. Fonfría, G. Quintana-Lacaci, C. Cabezas, C. Bermúdez, and M. Guélin, Astron. Astrophys. **627**, L4 (2019).
[13] H. Gupta, C. A. Gottlieb, V. Lattanzi, J. C. Pearson, and M. C. McCarthy, Astrophys. J. Lett. **778**, L1 (2013).
[14] J. Cernicharo, C. Cabezas, J. R. Pardo, M. Agúndez, C. Bermúdez, L. Velilla-Prieto, F. Tercero, J. A. López-Pérez, J. D. Gallego, J. P. Fonfría, G. Quintana-Lacaci, M. Guélin, and Y. Endo, Astron. Astrophys. **630**, L2 (2019).
[15] S. Petrie, Mon. Not. Roy. Astron. Soc. **282**, 807 (1996).
[16] K. Kawaguchi, E. Kagi, T. Hirano, S. Takano, and S. Saito, Astrophys. J. **406**, L39 (1993).
[17] P. Glarborg and P. Marshall, Energy Fuels **31**, 2156 (2017).
[18] M. Sarla, M. Pandit, D. K. Tyagi, and J. C. Kapoor, J. Hazard. Mater. **116**, 49 (2004).
[19] I. Fourré, O. Matz, Y. Ellinger, and J. C. Guillemin, Astron. Astrophys. **639**, A16 (2020).
[20] D. H. Quan, E. Herbst, Y. Osamura, and E. Roueff, Astrophys. J. **725**, 2101 (2010).
[21] N. Marcelino, S. Brünken, J. Cernicharo, D. Quan, E. Roueff, E. Herbst, and P. Thaddeus, Astron. Astrophys. **516**, A105 (2010).
[22] P. Gorai, B. Bhat, M. Sil, S. K. Mondal, R. Ghosh, S. K. Chakrabarti, and A. Das, Astrophys. J. **895**, 86 (2020).
[23] M. Ferus, D. Nesvorný, J. Šponer, P. Kubelík, R. Michalčíková, V. Shestivská, J. E. Šponer, and S. Civiš, Proc. Natl. Acad. Sci. USA **112**, 657 (2015).
[24] B. M. Rode, W. Kosmus, and E. Nachbaur, Chem. Phys. Lett. **17**, 186 (1972).
[25] D. Poppinger and L. Radom, J. Am. Chem. Soc. **100**, 3674 (1978).
[26] L. C. Ellingboe, A. M. R. P. Bopegedera, C. R. Brazier, and P. F. Bernath, Chem. Phys. Lett. **126**, 285 (1986).
[27] T. Pasinszki, T. Veszprémi, and M. Fehér, Chem. Phys. Lett. **215**, 395 (1993).
[28] T. Trabelsi, M. C. Davis, R. C. Fortenberry, and J. S. Francisco, J. Chem. Phys. **151**, 244303 (2019).
[29] Á. Vega-Vega, A. Largo, P. Redondo, and C. Barrientos, ACS Earth Space Chem. **1**, 158 (2017).
[30] J. Bai and H. T. Yu, New J. Chem. **46**, 7879 (2022).
[31] V. Lattanzi, S. Thorwirth, C. A. Gottlieb, and M. C. McCarthy, J. Phys. Chem. Lett. **3**, 3420 (2012).
[32] J. C. Choe, Astrophys. J. **914**, 136 (2021).
[33] R. L. Brown, Astrophys. J. **248**, L119 (1981).
[34] N. Marcelino, M. Agúndez, J. Cernicharo, E. Roueff, and M. Tafalla, Astron. Astrophys. **612**, L10 (2018).
[35] P. Redondo, M. Sanz-Novo, and C. Barrientos, Astrophys. J. **928**, 69 (2022).
[36] N. Mauron and P. J. Huggins, Astron. Astrophys. **513**, A31 (2010).
[37] X. Wu, L. L. Zhao, J. Y. Jin, S. Pan, W. Li, X. Y. Jin, G. J. Wang, M. F. Zhou, and G. Frenking, Science **361**, 912 (2018).
[38] L. N. Wang, S. Pan, G. J. Wang, X. Q. Zeng, M. F. Zhou, and G. Frenking, Chem. Commun. **58**, 8532 (2022).
[39] W. S. Drozdoski, A. P. Baronavski, and J. R. McDonald, Chem. Phys. Lett. **64**, 421 (1979).
[40] C. N. Filer and C. T. Peng, J. Labelled Compd. Radiopharm. **63**, 240 (2020).
[41] M. J. Frisch, J. A. Pople, and J. S. Binkley, J. Chem. Phys. **80**, 3265 (1984).
[42] A. P. Scott and L. Radom, J. Phys. Chem. **100**, 16502 (1996).
[43] M. Dolg, H. Stoll, and H. Preuss, J. Chem. Phys. **90**, 1730 (1989).
[44] M. Kaupp, P. V. R. Schleyer, H. Stoll, and H. Preuss, J. Chem. Phys. **94**, 1360 (1991).
[45] M. P. Andersson and P. Uvdal, J. Phys. Chem. A **109**, 2937 (2005).
[46] M. J. Frisch, G. W. Trucks, H. B. Schlegel, G. E. Scuseria, M. A. Robb, J. R. Cheeseman, G. Scalmani, V. Barone, G. A. Petersson, H. Nakatsuji, X. Li, M. Caricato, A. V. Marenich, J. Bloino, B. G. Janesko, R. Gomperts, B. Mennucci, H. P. Hratchian, J. V. Ortiz, A. F. Izmaylov, J. L. Sonnenberg, D. Williams-Young, F. Ding, F. Lipparini, F. Egidi, J. Goings, B. Peng, A. Petrone, T. Henderson, D. Ranasinghe, V. G. Zakrzewski, J. Gao, N. Rega, G. Zheng, W. Liang, M. Hada, M. Ehara, K. Toyota, R. Fukuda, J. Hasegawa, M. Ishida, T. Nakajima, Y. Honda, O. Kitao, H. Nakai, T. Vreven, K. Throssell, J. A. Mont-

DOI: 10.1063/1674-0068/cjcp2402019

gomery Jr., J. E. Peralta, F. Ogliaro, M. J. Bearpark, J. J. Heyd, E. N. Brothers, K. N. Kudin, V. N. Staroverov, T. A. Keith, R. Kobayashi, J. Normand, K. Raghavachari, A. P. Rendell, J. C. Burant, S. S. Iyengar, J. Tomasi, M. Cossi, J. M. Millam, M. Klene, C. Adamo, R. Cammi, J. W. Ochterski, R. L. Martin, K. Morokuma, O. Farkas, J. B. Foresman, and D. J. Fox, *Gaussian 16 Rev. C. 01*, Wallingford, CT: Gaussian Inc., (2016).

[47] R. F. W. Bader, *Atoms in Molecules: A Quantum Theory*, Oxford: Clarendon Press, (1990).

[48] T. A. Keith, *AIMAll, Version 17.11. 14*, Overland Park, KS, USA: TK Gristmill Software, (2017).

[49] E. D. Glendening, C. R. Landis, and F. Weinhold, J. Comput. Chem. **34**, 1429 (2013).

[50] A. Michalak, M. Mitoraj, and T. Ziegler, J. Phys. Chem. A **112**, 1933 (2008).

[51] M. P. Mitoraj, A. Michalak, and T. Ziegler, J. Chem. Theory Comput. **5**, 962 (2009).

[52] L. L. Zhao, M. von Hopffgarten, D. M. Andrada, and G. Frenking, WIREs Comput. Mol. Sci. **8**, e1345 (2018).

[53] L. L. Zhao, M. Hermann, W. H. E. Schwarz, and G. Frenking, Nat. Rev. Chem. **3**, 48 (2019).

[54] *ADF2014, SCM, Theoretical Chemistry*, Amsterdam, The Netherlands: Vrije Universiteit, https://www.scm.com.

[55] G. te Velde, F. M. Bickelhaupt, E. J. Baerends, C. Fonseca Guerra, S. J. A. van Gisbergen, J. G. Snijders, and T. Ziegler, J. Comput. Chem. **22**, 931 (2001).

[56] E. Van Lenthe and E. J. Baerends, J. Comput. Chem. **24**, 1142 (2003).

[57] G. J. Wang and M. F. Zhou, Int. Rev. Phys. Chem. **27**, 1 (2008).

[58] C. A. Thompson, L. Andrews, J. M. L. Martin, and J. El-Yazal, J. Phys. Chem. **99**, 13839 (1995).

[59] L. N. Wang, S. Pan, B. Lu, X. L. Dong, H. M. Li, G. H. Deng, X. Q. Zeng, M. F. Zhou, and G. Frenking, Angew. Chem. Int. Ed. **60**, 4518 (2021).

[60] M. F. Zhou and L. Andrews, J. Am. Chem. Soc. **120**, 11499 (1998).

[61] M. D. Leslie, M. Ridoli, J. G. Murphy, and N. Borduas-Dedekind, Environ. Sci.: Processes Impacts **21**, 793 (2019).

[62] P. Pyykkö and M. Atsumi, Chem. Eur. J. **15**, 12770 (2009).

[63] P. Redondo, A. Largo, and C. Barrientos, Astrophys. J. **899**, 135 (2020).

DOI: 10.1063/1674-0068/cjcp2402019